Version of Record: https://www.sciencedirect.com/science/article/pii/S0376738824000590
Manuscript_00caf51deafbed1721f9e7c342b2e970

Elucidating the role of micropore-generating backbone motifs and amine functionality on H_2S, CO_2, CH_4 and N_2 sorption

Pablo A. Dean[1], Katherine Mizrahi Rodriguez[2*], Sheng Guo[3], Naksha Roy[1], Timothy M. Swager[3], and Zachary P. Smith[1†]*

[*]*Co-first authors*

[†]*Corresponding author: zpsmith@mit.edu.*

[1]Department of Chemical Engineering, Massachusetts Institute of Technology, 77 Massachusetts Avenue, Cambridge, MA 02139, USA.

[2]Department of Materials Science and Engineering, Massachusetts Institute of Technology, 77 Massachusetts Avenue, Cambridge, MA 02139, USA.

[3]Department of Chemistry, Massachusetts Institute of Technology, 77 Massachusetts Avenue, Cambridge, MA 02139, USA.

Keywords

Polymers of intrinsic microporosity, backbone functionality, amines, sorption energetics.

© 2024 published by Elsevier. This manuscript is made available under the Elsevier user license
https://www.elsevier.com/open-access/userlicense/1.0/

Abstract

Microporous polymers have transformed the field of membrane-based gas separations over the past two decades. However, applying sorbent materials as membranes presents a unique challenge in quantifying emergent phenomena, such as how strongly sorbing penetrants influence transport of co-permeating species. These mechanistic features are of urgent concern for many current and emerging applications, yet they remain significantly understudied. In previous work, amine-functionalized PIM-1 (PIM-NH_2) has proven to be an exemplar of these effects, exhibiting CO_2/CH_4 mixed-gas selectivities that are 2.6 times higher than selectivities calculated from pure-gas measurements. Here, we investigate the generalizability of this sorption-induced emergent phenomena through the synthesis of a novel amine-functional microporous poly(arylene ether) (PAE-NH_2). The effects of amine functionalization on gas transport were analyzed through variable-temperature pure-gas sorption tests, ternary mixed-gas sorption modeling, and dual-mode sorption analysis for N_2, CH_4, CO_2, and H_2S. Compared to its nitrile-functional counterpart (PAE-CN), pure-gas sorption for PAE-NH_2 was 69% higher for CO_2 and 26% higher for H_2S at 1 atm and 35 °C, suggesting increased affinity to both CO_2 and H_2S. However, the higher total sorption for H_2S resulted in strong competitive sorption effects, decreasing permeability of both CO_2 and CH_4 for mixture experiments, which was reported in our complementary study on the mixed-gas separation performance of the same materials in this work. The strength of gas–polymer interactions were quantified by evaluating experimental isosteric heats of sorption for the acid gases in PIM-1, PIM-NH_2, PAE-CN, and PAE-NH_2. Amine-functionalized samples showed highly exothermic interactions, with minima in isosteric heats of approximately −44 kJ mol^{-1} for CO_2 and −34 kJ mol^{-1} for H_2S. Leveraging

51 microporosity and amine-functionality in membranes are general approaches to access
52 competitive sorption for many industrially relevant gas separations.

53 **1. Introduction**

54 With the highest heating value per unit mass (55.5 MJ/kg) of all hydrocarbon fuels,
55 methane will likely remain an attractive option for meeting the world's ever-growing energy
56 demands.[1] At the same time, using other renewable sources of methane has become vital in
57 promoting a sustainable future. In particular, renewable natural gas (RNG) derived from biogas
58 and landfill gas has emerged as a promising source of methane from unavoidable waste streams,
59 such as dairy farms and wastewater treatment plants.[2] The utilization of renewable natural gas
60 and other lower-quality reserves, however, requires separation technology to remove hydrogen
61 sulfide (H_2S) and CO_2 in order to meet industrial pipeline specifications (i.e., H_2S concentrations
62 under 4 ppm and CO_2 concentrations between 2 mol% and 4 mol%).[3] In natural gas reservoirs,
63 H_2S ranges in concentration from parts-per-million (ppm) to 30 mol% in parts of the Middle
64 East.[4,5] Conventional absorption and cryogenic distillation processes used for extracting H_2S
65 have high energy demands that limit their implementation.[3] Membrane-based separation systems
66 offer an energy- and space-efficient alternative for a more sustainable production of methane
67 resources.[6]

68 Polymeric membranes are attractive for sour-gas (CO_2, H_2S) separations due to
69 complementary diffusion- and sorption-selective transport. This feature results from the relative
70 size and condensability of relevant diluents, where CO_2 and H_2S are both smaller and more
71 condensable than CH_4, resulting in favorable size-sieving and partitioning of the acid gases.
72 When considering H_2S/CH_4 separations, however, the difference in kinetic diameters of H_2S
73 (3.62 Å) and CH_4 (3.80 Å) is much smaller than the difference between CO_2 (3.30 Å) and CH_4

(3.80 Å), so the complexity of a ternary $H_2S/CO_2/CH_4$ system requires additional interpretational nuance to evaluate how co-permeating acid gases influence transport. While traditional rubbery polymers (e.g., PDMS) are suited for sorption-driven separations because of their diminished ability to separate gases based on size,[6] the advent of functionalized microporous polymers has resulted in materials with impressive simultaneous sorption and diffusion selectivities, and, as a result, high combined acid-gas selectivity ($(CO_2+H_2S)/CH_4$). Such polymers include amidoxime-functionalized polymers of intrinsic microporosity (AO-PIM-1)[7] and hydroxyl-containing PIM-6FDA-OH,[8] but many other polymer compositions within the microporous polymer subclass remain underexplored.

Therefore, there is a pressing need to expand research efforts in materials discovery of microporous polymers, but of equal importance, emergent transport phenomena arising from these systems needs to be understood and leveraged to update theory and improve separation systems. For acid-gas separations, microporous polymers can benefit from competitive sorption effects as long as penetrant-induced swelling is mitigated. Competitive sorption is the phenomenon where more condensable diluents (i.e., CO_2 and H_2S) exclude less condensable species (i.e., CH_4 and N_2) from the polymer matrix, resulting in higher sorption selectivity compared to pure-gas tests. However, leveraging this increase in sorption selectivity while maintaining high diffusion selectivity is difficult in the presence of strongly sorbing gases like H_2S ($T_c = 373.5\,K$), which can plasticize the polymer, a phenomenon marked by increased mobility of polymer chains at high pressures that reduces size-sieving ability.

Evaluating competitive sorption is important for designing membrane materials intended for the purification of industrially relevant gas mixtures. While a large component of membrane characterization relies on pure-gas measurements, these are often poor predictors of performance

97 at realistic operating conditions, where condensable gases like H_2S and CO_2 can severely alter
98 the selectivity of a material.[9,10] The deviation between pure- and mixed-gas performance is often
99 substantial, especially for gas pairs that exhibit large differences in condensability.[11,12] CO_2/CH_4
100 separations are a good example of this phenomenon, where mixed-gas sorption experiments have
101 demonstrated that CO_2 can exclude CH_4 from the polymer.[13,14] This exclusion increases CO_2-
102 based sorption selectivity in mixed-gas conditions, and has been shown to increase mixed-gas
103 selectivity relative to the pure-gas case.[15] In fact, due to the marked difference between pure- and
104 mixed-gas performance for a number of polymers, in 2018 Wang et al. constructed an empirical
105 permeability–selectivity upper bound tradeoff that compares data from mixed-gas permeation
106 tests with those of standard pure-gas tests.[16] While the prevailing view in the field is that
107 plasticization effects will adversely impact stability,[17–19] resulting in a deterioration in separation
108 performance, the advent of applying microporous polymers to these separations and the
109 possibility of leveraging competitive sorption cannot be ignored.
110 Although mixed-gas sorption experiments are a useful tool in understanding competition
111 in gas mixtures, these tests are difficult to conduct,[13,14] which has necessitated the use of models
112 to predict mixed-gas sorption coefficients based on accessible pure-gas sorption data. One such
113 phenomenological model is the dual-mode sorption (DMS) model, which can be modified to
114 account for the presence of multiple components in a mixture.[20] Due to its ease of
115 implementation and widespread use in membrane literature,[21] this model is an appropriate choice
116 for analyzing mixed-gas sorption in new materials, such as those that will be discussed in this
117 work. Additionally, the DMS model can be applied to predict multi-temperature sorption
118 isotherms for mixtures even when mixture sorption data are unavailable. These data and the
119 corresponding extraction of isosteric heats of sorption (ΔH_I) provide quantifiable energetic

values that enable comparison between the affinity of a polymer for one gas over another, and also provide insights into the effects of polymer microstructure on sorption within the DMS framework.[21] Taken together, mixed-gas sorption modelling and sorption energetic analysis are useful in elucidating the effects of polymer microstructure and chemical composition on competitive sorption effects in sour-gas mixtures.

Previous work has focused on maximizing CO_2/CH_4 and H_2S/CH_4 separation performance simultaneously in polymer membranes. In 1997, poly(propylene oxide)- and poly(ethylene oxide)-derived polyurethanes showed impressive CO_2/CH_4 and H_2S/CH_4 selectivities of 15–20 and 66–95, respectively, indicating that polyether content is favorable for H_2S-focused separations.[22,23] Highly permeable polymers, including rubbery polydimethylsiloxane (PDMS) and glassy poly[1-(trimethylsilyl)-1-propyne] (PTMSP) were also studied in 2001 and showed high H_2S permeabilities of 5100 and 21400 barrer, respectively.[23] In 2013, researchers also began to investigate the glassy polyimides 6FDA-DAM and 6FDA-DAM:DABA for H_2S separations. The DABA variant contains a carboxylic acid group, which could be crosslinked to improve stability in the presence of H_2S.[24,25] Fluorinated poly(amide-imide) (PAI) membranes have also been studied in binary and ternary mixtures, but these materials were shown to be susceptible to H_2S plasticization.[26] While these previous studies have demonstrated exciting results based on permeation, questions remain on how sorption properties, specifically H_2S sorption, influences the co-permeating species, and, by extension, how H_2S sorption is related to polymer architecture, a crucial relationship for designing new membrane materials. In response, this study correlates H_2S sorption with the structure and functionality of a new amine-functionalized microporous polymer backbone.

142 The modification of polymer membranes via functionalization or crosslinking has shown
143 promise in enhancing separations with H_2S. Previously, structural modifications were
144 investigated for cellulose acetate (CTA) since the native material exhibits moderate selectivity
145 and low gas permeability relative to many other polymers. One approach involved silane grafting
146 and crosslinking with vinyltrimethoxysilane, and the resultant material achieved higher H_2S
147 permeability (190 vs 39.7 barrer) than untreated CTA.[27] The silane groups serve to increase free
148 volume, and crosslinking stabilized the polymer against plasticization. Unmodified CTA was
149 also studied in industrially relevant hollow fiber membranes with ~200-nm-thick selective layers,
150 achieving high CO_2 and H_2S permeances (113.5 and 144.7 GPU, respectively) and CO_2/CH_4 and
151 H_2S/CH_4 selectivities of 22 and 28, respectively.[28] Given their high permeabilities and H_2S/CH_4
152 selectivities, the Pebax® family of materials makes use of glassy polyamide and rubbery
153 polyether blocks and has exhibited promising separation performance relative to the reported
154 sour-gas upper bounds.[29] Despite the progress in performance metrics, little is known about H_2S
155 sorption and sorption energetics in these materials. Studying H_2S sorption in membranes would
156 help to deconvolute the effects of diffusion and sorption on separation performance and inform
157 the development of functionalization strategies to increase affinity for acid gases.
158 Polymers of intrinsic microporosity (PIMs) have gained traction for sour-gas separations
159 due to their ultrahigh permeability and high internal surface area.[30] However, only a few PIMs
160 have been studied for H_2S-related applications, including PIM-1, a hydroxyl-functionalized
161 PIM–polyimide, and an amidoxime-functionalized PIM-1 (AO-PIM-1).[7,8] With these materials,
162 high H_2S permeabilities up to 17100 barrer were achieved, and AO-PIM-1 exhibited CO_2/CH_4
163 and H_2S/CH_4 selectivities of 14.7 and 75.1, respectively.[7] The hydroxyl-functionalized PIM–
164 polyimide showed reasonable selectivities of 25 and 30 for CO_2/CH_4 and H_2S/CH_4, respectively.[8]

These high selectivities can be attributed to the hydrogen bonding between the acid gases and the –OH groups present on the polymer backbone, leading to increased sorption selectivities. Although H_2S sorption isotherms have been collected for some of these microporous materials, these studies do not analyze sorption energetics, which can provide key fundamental insights into the relationship between gas–polymer affinity and polymer architecture. Other functional groups such as the primary amine have been investigated for acid-gas removal, primarily focusing on CO_2/CH_4 binary mixtures. Previous work by our group investigated the separation performance of amine-functionalized PIM-1 (PIM-NH_2) and other functionalized PIM-1 analogues in binary CO_2-based mixtures.[31] PIM-NH_2 showed the largest enhancement in CO_2/CH_4 selectivity in mixed-gas conditions relative to the pure-gas case.[31] This unusual performance improvement was explained by the exclusion of CH_4 from the polymer matrix by CO_2, and mixed-gas CO_2 and CH_4 sorption predictions were used to validate this claim.

In this work, we investigate the generalizability of our previous work regarding amine-boosted acid-gas sorption by developing an amine-functionalized polymer based on a newly reported poly(arylene ether) backbone (PAE) architecture.[32,33] Using a post-synthetic functionalization procedure, a nitrile-containing PAE (PAE-CN) was modified into its primary-amine-functionalized counterpart (PAE-NH_2). To elucidate the sorption mechanisms influencing acid-gas transport in these amine-containing materials, we investigated variable-temperature pure-gas sorption for CO_2, N_2, CH_4 and H_2S at 35 °C, 45 °C, 55 °C, and 65 °C. Using an optimized constrained dual-mode sorption (DMS) fitting analysis developed by Wu et al.,[21] we extract high-precision DMS parameters from these data as well as details on sorption energetics for all gases. Transport theory and the extension of the DMS model to mixtures are used to predict ternary mixed-gas sorption and calculate isosteric heats of sorption, revealing

fundamental insights to inform the future design of microporous materials for sour-gas applications.

2. Background and Theory

Gas transport in polymers is often described by the sorption–diffusion model[34]:

$$P = D \times S \tag{1}$$

where P is the permeability or the pressure- and thickness- normalized flux through a film in units of barrer (10^{-10} cm^3_{STP} $cm^{-3}_{polymer}$ cm^2 $cmHg^{-1}$ s^{-1}), D is the concentration-averaged diffusion coefficient (cm^2 s^{-1}), and S is the sorption coefficient (cm^3_{STP} $cm^{-3}_{polymer}$ $cmHg^{-1}$). Changes in backbone rigidity and polymer packing structure will influence transport performance primarily through changes in the diffusion coefficient, while changes in chemical functionality and gas–polymer interactions will influence performance primarily through changes in the sorption coefficient, which can be measured directly through sorption experiments. In glassy polymers, pure-gas sorption isotherms are often described through the dual-mode sorption (DMS) model[35,36]:

$$C_{i,\mathrm{pure}} = k_{\mathrm{D},i} f_i + \frac{C'_{\mathrm{H},i} b_i f_i}{1 + b_i f_i} \tag{2}$$

where C_i is the concentration of gas i in the polymer (cm^3_{STP} cm^{-3}_{pol}), $k_{\mathrm{D},i}$ is the Henry's law constant (cm^3_{STP} cm^{-3}_{pol} atm^{-1}), $C'_{\mathrm{H},i}$ is the Langmuir sorption capacity (cm^3_{STP} cm^{-3}_{pol}), b_i is the Langmuir affinity constant (atm^{-1}), and f_i is the equilibrium fugacity (atm). DMS parameters are often fitted using a nonlinear optimization with or without

211 constraints. However, Ricci et al. demonstrated how unconstrained DMS fittings can
212 result in multiple solutions with little physical meaning.[37] In this work, DMS parameters
213 were calculated using a precise nonlinear optimization method developed by Wu et al.[21]
214 This method applies van't Hoff and linear free energy relationship (LFER) constraints to
215 the thermodynamically-based constants, k_D and b, and an additional constraint that C'_H
216 decreases with temperature. Parameter optimizations were run by minimizing the χ^2
217 objective function in MATLAB. Uncertainties were calculated through error propagation
218 or χ^2 parabolic estimation.[38] The lower and upper bounds on constraints used for the
219 MATLAB optimization are tabulated in **Tables S2–3**.

220 In 1981, Koros et al. developed an extension of the DMS model to enable
221 predictions of mixed-gas sorption isotherms.[20] This extension assumes that the
222 equilibrium mode of sorption is not affected by the presence of other penetrants in a
223 binary or ternary mixture, and the application of this model has been useful for predicting
224 the behavior of gas sorption in mixtures when mixed-gas sorption experiments are not
225 accessible.[39,40] For a ternary mixture, for instance, the pure-gas Langmuir affinity constant
226 for the other penetrants in the mixture (i.e., penetrants j and k) can be used to predict
227 mixed-gas sorption for the third penetrant (i):

228 $$C_{i,\text{mixed}} = k_{D,i} f_i + \frac{C'_{H,i} b_i f_i}{1 + b_i f_i + b_j f_j + b_k f_k} \quad (3)$$

229 Thus, the mixed-gas sorption coefficients and sorption selectivities can be calculated from the
230 pure-gas data, and they provide a measure of sorption with respect to pressure or fugacity using
231 the following equations:

232 $$S_i = \frac{C_i}{f_i} \quad (4)$$

$$\alpha_{i/j}^{S} = \frac{S_i}{S_j} = \frac{C_i}{f_i} / \frac{C_j}{f_j} \quad (5)$$

In addition to these pressure-dependent sorption parameters that are calculated from the secant of a given isotherm, sorption isotherms can also be used to estimate sorption at infinite dilution (S_{inf}). The parameter S_{inf} is a measure of the affinity of the first gaseous diluent to partition into the polymer. In the limit of zero pressure or fugacity, S_{inf} is:

$$\lim_{f \to 0} S = k_{\text{D}} + C'_{\text{H}} b = S_{inf} \quad (6)$$

When considering multiple temperatures, the temperature dependence of S, k_{D}, and b can be represented as van't Hoff expressions[21,41–43]:

$$S = S_0 \exp\left(-\frac{\Delta H_{\text{S}}}{RT}\right) \quad (7)$$

$$k_{\text{D}} = k_{\text{D},0} \exp\left(-\frac{\Delta H_{\text{D}}}{RT}\right) \quad (8)$$

$$b = b_0 \exp\left(-\frac{\Delta H_{\text{b}}}{RT}\right) \quad (9)$$

where ΔH_{S}, ΔH_{D}, and ΔH_{b} are the overall heat of sorption (kJ mol^{-1}), the enthalpy of Henry sorption (kJ mol^{-1}), and the enthalpy of Langmuir sorption (kJ mol^{-1}), respectively, and S_0 (cm$^3_{\text{STP}}$ cm$^{-3}_{\text{pol}}$ atm^{-1}), $k_{\text{D},0}$ (cm$^3_{\text{STP}}$ cm$^{-3}_{\text{pol}}$ atm^{-1}), and b_0 (atm^{-1}) are pre-exponential factors.

Using sorption isotherms at various temperatures, the isosteric heats of sorption can be calculated to elucidate the dependence of the heat of sorption with penetrant concentration[42]:

$$\left[\frac{d \ln p}{d\,(1/T)}\right]_C = \frac{\Delta H_{\text{I}}}{zR} \quad (10)$$

where ΔH_{I} is the enthalpy of sorption at a concentration C, p is the equilibrium pressure for each data point, and z is the compressibility factor for the gas.

3. Results

3.1. Chemical characterization

As shown in the schematic in **Figure 1a**, PIM-1 and PAE-CN were post-synthetically functionalized with a primary amine ($–CH_2NH_2$).[44] In prior work by Mason et al., amine-functionalization of PIM-1 powder or films was conducted using a borane–dimethyl sulfide complex in THF or diethyl ether. The amine-functionalized PIM-1 (PIM-NH_2) became an insoluble product in common solvents. Herein, we extend the functionalization strategy to a nitrile-functionalized PAE polymer composed of the spirobifluorene unit and a triptycene moiety. As shown in **Figure S2**, powder samples of PAE-CN were post-synthetically functionalized using either a THF or diethyl ether-based borane–dimethyl sulfide complex for five hours. In all cases, the products were insoluble in common laboratory solvents. The functionalization strategy was extended to solid-state films using the dimethyl sulfide non-solvent. The PAE-based films and powder were characterized through FT-IR and solid-state NMR analysis, as shown in **Figure 1** and **Figure S2**, respectively. Previously reported spectra for PIM-1 and PIM-NH_2 are included for comparison.[45] The FT-IR spectra for PIM-1 and PAE-CN show the characteristic stretches for a nitrile group at 2239 cm^{-1} and 2228 cm^{-1}, respectively, which are absent in PIM-NH_2 and PAE-NH_2, indicating successful functionalization of the –CN. PAE-NH_2 samples also show new signals for the –NH wag at 807 cm^{-1} and the –NH stretch centered at approximately 3350 cm^{-1}, in accordance with the chemical features previously observed for PIM-NH_2.[44,45] A closer view of the –NH stretch is provided in **Figure S3**.

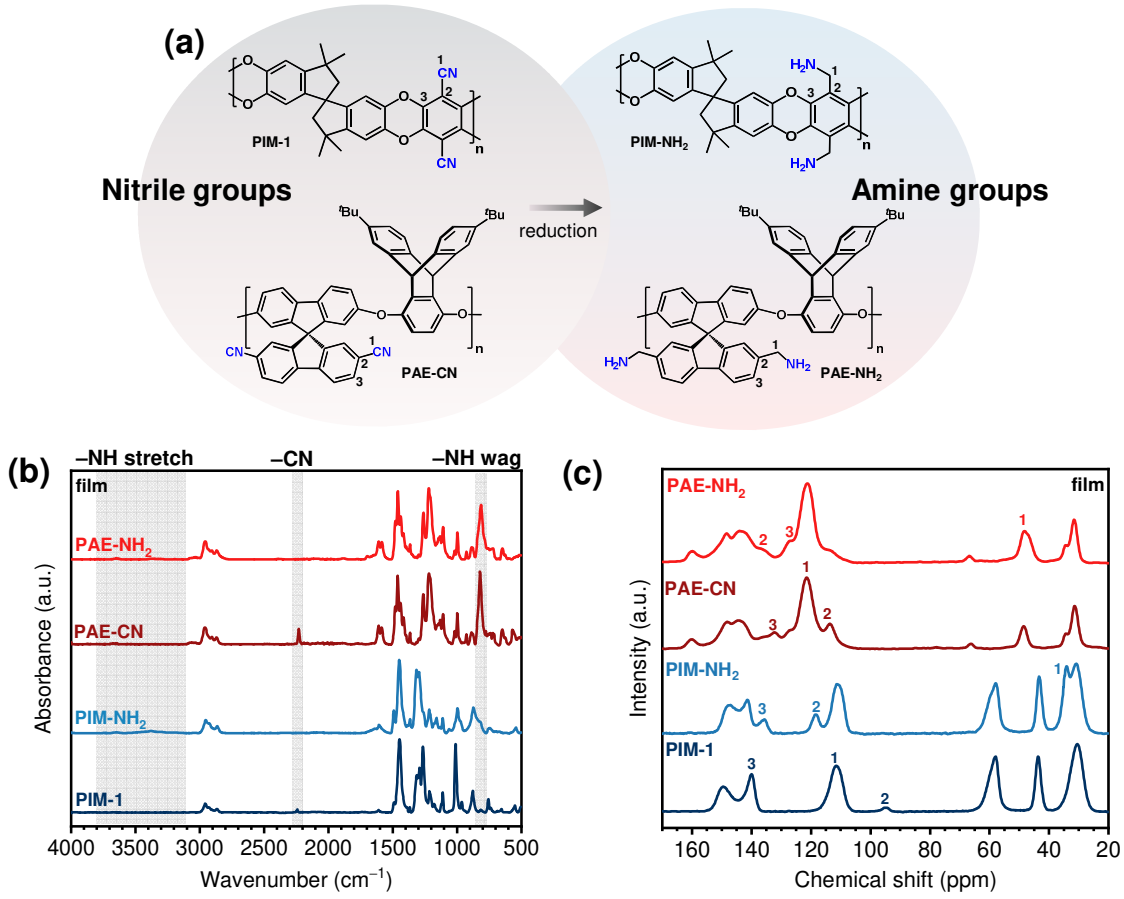

273

274 **Figure 1.** (a) Chemical structures, (b) FT-IR spectra, and (c) solid-state NMR spectra for PIM-1,
275 PAE-CN, PIM-NH_2, and PAE-NH_2.

276 The samples were further characterized through MAS solid-state ^{13}C NMR, as shown in
277 **Figure 1c and S2c**. The solid-state NMR spectra for the PAEs are composed of many broad
278 peaks between 110 and 160 ppm, which correspond to various aromatic carbons with small
279 differences in chemical shift. Because PAE-CN is soluble in chloroform, some of these key
280 peaks can be resolved by solution-state NMR and HSQC, COSY, HMBC, and DEPT-135 NMR
281 spectra, which are also shown in **Figure S1**. When comparing the solid-state spectra for PAE-CN

and PAE-NH_2, the chemical shifts show three primary differences. First, the signal at 132 ppm, which is associated with the aromatic carbon adjacent to the functional moiety, shifts upfield to 126 ppm. Second, the chemical signal at 113 ppm, which is associated with the aromatic carbon directly attached to the –CN, significantly reduces in intensity and appears at a new chemical shift of 136 ppm in PAE-NH_2. Finally, the carbon signal for the –CN group, which is potentially concealed in the large peak at 121 ppm, shifts upfield and likely merges with another peak to form a broad signal at 47 ppm. These chemical shift changes mirror those observed when functionalizing PIM-1 to PIM-NH_2 and indicate successful amine-functionalization of PAE-CN.

The thermal profiles and stability of the four polymer samples were characterized through thermogravimetric analysis in an inert atmosphere as shown in **Figure S4**. Similar to PIMs, the PAEs show excellent thermal stability up to 500 °C, where the onset of backbone decomposition affiliated with the breakage of ether linkages becomes apparent.[46] Compared to the two PIMs, PAE analogues generally show enhanced thermal stability. The temperatures required to lose 5% mass (TD-5) for PAE-CN and PAE-NH_2 are each 493 °C, whereas PIM-1 and PIM-NH_2 exhibit TD-5 values of 489 °C and 444 °C, respectively. The enhanced thermal stability of PAEs may result from the high stability of the SBF and triptycene monomers, which do not contain chemically labile bonds for decomposition. This finding represents an interesting feature for potential carbonization of PAE samples into carbon molecular sieving materials, which often benefit in terms of mechanical properties if they have low mass loss during carbonization.[47,48] When considering the amine-functionalized analogues, both PIM-NH_2 and PAE-NH_2 show a higher decomposition rate between 425–465 °C, which was associated with the degradation of the –NH_2 functionality at these temperatures.

3.2. Physical characterization

While the PAE backbones considered here contain tert-butyl, triptycene, and SBF functionalities with high configurational free volume, the linear ether backbone connectivity allows for more segmental flexibility in comparison to the rigid ladder structure of PIM-1. Thus, there is a tradeoff that must be considered between the enhanced configurational free volume based on polymer composition and the increased backbone flexibility that can lead to denser polymer packing structures. Related tradeoffs in polyimides have been highlighted in work by the Guo and Freeman groups, where triptycene-based polyimides with ether linkages were shown to have lower permeabilities than those without ether linkages.[49–51] In accordance with this behavior, the BET surface area for PIM-1 is usually reported at approximately 800 m^2g^{-1},[45,52] whereas that of PAE-CN is 288 m^2g^{-1} (**Figure S5**), which follows the expected trends for permeability,[53,54] which will be reported later. We pause briefly to acknowledge an ongoing debate in the literature on the quantitative nature of applying BET analysis to polymers of intrinsic microporosity.[55,56] However, given the long-standing precedent for using BET on microporous polymers,[55] and thus, the vast amount of comparable literature data, we report the BET surface area as a useful comparison point for previously studied microporous polymers.

To further evaluate the role of free volume in this comparative study, the PAEs and PIMs were characterized for density. The densities of PIM-1 and PIM-NH_2 have been previously reported and are very close to that of water, making standard density measurements from aqueous buoyancy measurements challenging.[45] Perhaps because of this challenge and because of the high non-equilibrium free volume of PIM-1, density measurements have shown large variability in the literature.[57] To address these uncertainties, buoyancy measurements were conducted in this study with three high molecular weight hydrocarbons that have significantly

lower densities than water: heptane ($MW = 100.21$ g mol $^{-1}$, 0.68 g cm^{-3}), decane ($MW = 142.29$ g mol^{-1}, 0.73 g cm^{-3}), and hexadecane ($MW = 226.41$ g mol^{-1}, 0.77 g cm^{-3}). As the molecular weight of the buoyant fluid increases, liquid diffusion into the polymer matrix is expected to decrease, as can be gleaned from vapor sorption experiments for PIM-1 using pentane, hexane, and heptane.[58] Because hydrocarbon sorption into these polymers can potentially influence density measurements, we investigated larger buoyant fluids to slow down this kinetic effect. In **Figure S6**, as the buoyant fluid molecular weight increases, the density appears to plateau to the real bulk density value. Density measurements for PIM-NH_2, PAE-CN, and PAE-NH_2 remain within the uncertainty of the measurement for all three solvents, but the apparent PIM-1 density steadily decreases with increasing solvent molecular weight from heptane to decane and then plateaus for hexadecane. This result correlates with the higher permeabilities of PIM-1, suggesting that lower molecular weight hydrocarbons like heptane sorb more rapidly in this polymer compared to other samples. Thus, the densities in hexadecane were selected as the most suitable values for analysis of fractional free volume (FFV) via group contribution methods, which are summarized in **Table S1.** FFV was calculated using van der Waals volumes reported by Park and Paul[59] and the modified group contribution method recently developed by Wu et al.[57] FFV calculated from the Wu method tends to be higher for both PIMs and PAEs compared to calculations from the Park and Paul method, which is consistent with the trends observed for microporous materials using the updated method.[57] Moreover, the FFV calculated from the Wu method decreases by 7% from PIM-1 to PIM-NH_2 and by 29% from PAE-CN to PAE-NH_2. These decreases in FFV were attributed to densification in the polymer structure due to the addition of hydrogen bonding amines. The larger decrease in the FFV for PAEs is also potentially associated to their backbone flexibility derived from the ether linkages.

Moreover, there is a 48% decrease in FFV from PIM-1 to PAE-CN, which is in line with the 67% decrease in BET surface area.

WAXS spectra for PIM-1, PIM-NH_2, PAE-CN and PAE-NH_2 are illustrated as intensity, I, versus the scattering vector, $q = 4\pi(\sin\theta)/\lambda$, in **Figure S7**, where λ is the wavelength of the X-ray beam and θ is Bragg's angle. Characteristic signals for PIM-1 and PIM-NH_2 have been previously discussed,[45,60] where the three signals at large scattering vectors represent inter-segmental spacing between polymer chains. The WAXS pattern for PAE-CN and PAE-NH_2 show two amorphous halos at 0.49 and 1.22 $Å^{-1}$, which correspond to distances of 12.82 and 5.15 Å. These d-spacings may be attributed to SBF and triptycene, respectively. Previous work by Corrado et al. has ascribed configurational free volume to the triptycene moiety in triptycene-based polysulfones, with d-spacing in the range of 4.7 to 5.1 Å. Of note, chain-packing simulations of SBF-based PIMs has been performed by Bezzu et al.[61] In their study, simulated structures were used to derive cumulative pore volumes for characteristic PIMs such as PIM-SBF-1, where a broad halo at pore diameters between 3–6 Å was consistently observed, and may be representative of the characteristic peaks also observed in the PAE spectra. Of note, there were minimal differences in the WAXS spectra for PAE-CN and PAE-NH_2 suggesting that the large features in the WAXS patterns are indicative of structural characteristics present in both polymer backbones regardless of post-synthetic functionalization.

3.3. Pure gas sorption and sorption energetics

3.3.1. Sorption trends and correlations for various gases

N_2, CH_4, CO_2, and H_2S sorption isotherms tested at 35 °C for PIM-1, PIM-NH_2, PAE-CN, and PAE-NH_2 are presented in **Figures 2**, **S8**, and **S9**. These plots show the concave curvature characteristic of dual-mode sorption in glassy polymers.[43,62] For the supercritical gases

(i.e., N_2 and CH_4), PAE-CN and PAE-NH_2 have identical sorption curves while PIM-1 generally has higher sorption than PIM-NH_2. These differences are attributed primarily to the effect of Langmuir capacity on sorption of less polarizable gases, which will be discussed in detail later. For condensable gases (i.e., CO_2 and H_2S), amine-functionalized polymers have higher sorption capacity than the nitrile-functionalized analogues, suggesting favorable interactions between the amine and both CO_2 and H_2S. Notably, PIM-NH_2 retains higher total H_2S and CO_2 sorption than PIM-1 despite the inverse trend in N_2 and CH_4 sorption noted previously. Moreover, at 35 °C and 9.7 atm, the films reached remarkably high H_2S concentrations of 180, 200, 135 and 156 $cm^3_{STP}\,cm^{-3}_{pol}$ for PIM-1, PIM-NH_2, PAE-CN, and PAE-NH_2, respectively.

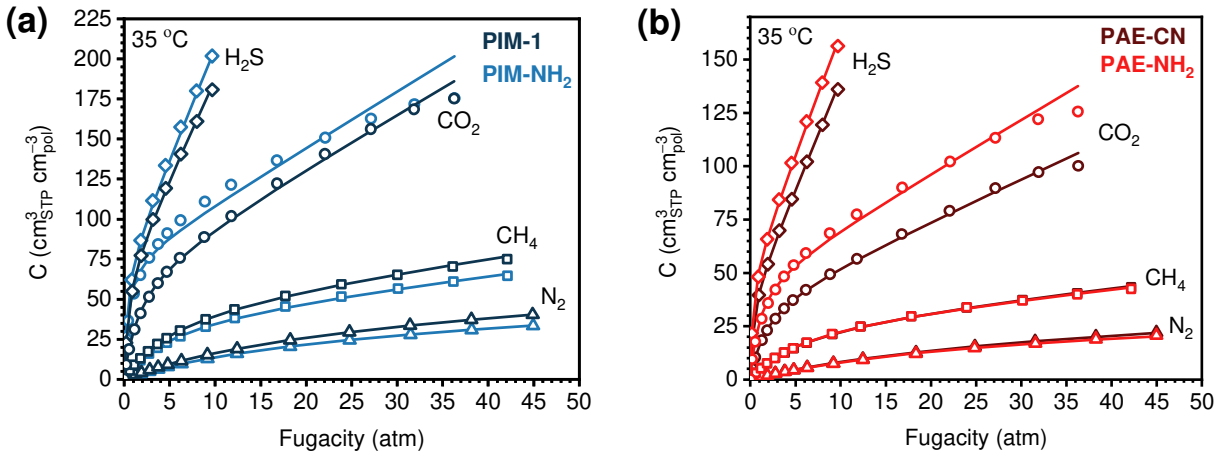

Figure 2. N_2, CH_4, CO_2, and H_2S sorption isotherms for (a) PIM-1 (dark blue) and PIM-NH_2 (light blue), and (b) PAE-CN (dark red) and PAE-NH_2 (light red) measured at 35 °C.

3.3.2. Dual-mode model fitting and interpretation

Sorption isotherms were collected at 35 °C, 45 °C, 55 °C, and 65 °C, permitting the application of a constrained dual-mode sorption fitting method previously developed by Wu et al.[21] H_2S isotherms for PIM-NH_2 and PAE-NH_2 at the four testing temperatures are shown in **Figure 3a and b**. All isotherms show the expected decrease in sorption with increasing

temperature.[43] Analogous plots for N_2, CH_4, CO_2 and H_2S sorption at variable temperatures for PIM-1, PIM-NH_2, PAE-CN, and PAE-NH_2 are summarized in **Figures S10–13**. The aforementioned fitting was performed to derive temperature-dependent DMS parameters and gain a phenomenological understanding of sorption of each gas in the four polymers considered.[20] Upper and lower bound constraints and initial guesses for the fittings are shown in **Tables S2–3**, and an example LFER for CH_4 sorption in PIM-1 is shown in **Figure S14**. DMS parameters and S_{inf} values measured at 35 °C, 45 °C, 55 °C, and 65 °C are reported in **Tables S4–7**.

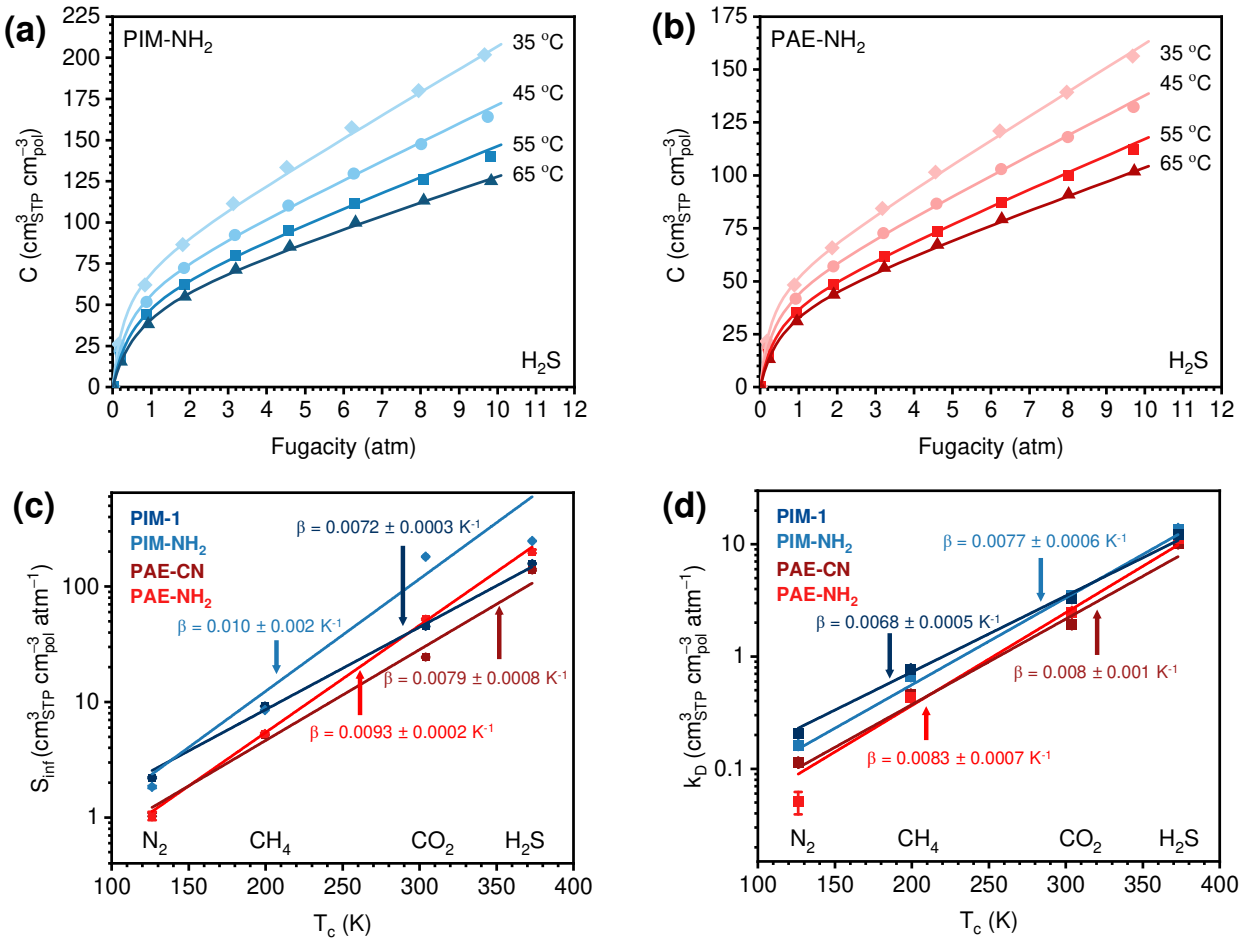

Figure 3. H_2S pure-gas sorption isotherms as a function of pressure at 35 °C (diamonds), 45 °C (circles), 55 °C (squares), and 65 °C (triangles) for (a) PIM-NH_2 and (b) PAE-NH_2. Sorption trends for (c) S_{inf} and (d) k_D versus critical temperature for PIM-1 (dark blue), PIM-NH_2 (light blue), PAE-CN (dark red), and PAE-NH_2 (light red). Slopes (β) and error for the fitted lines were calculated using the LINEST function in Excel.

Parameters derived from sorption fittings, such as S_{inf}, k_D, and b, are often correlated with measures of gas penetrant condensability such as critical temperature (T_c) and Lennard-Jones parameters (ε/κ).[63] The corresponding trends with T_c are shown in **Figure 3c and d** and **Figure S15.** The sorption at infinite dilution (S_{inf}) can be calculated from DMS parameters

according to **Equation 6** and provides a measure of intrinsic sorption into the polymer in the limit of zero pressure. For S_{inf} with respect to T_c, the polymers PIM-1, PIM-NH_2, PAE-CN, and PAE-NH_2 had slopes (β) of $0.010 \pm 0.002\ K^{-1}$, $0.0072\ \pm 0.003\ K^{-1}$, $0.0079\ \pm 0.0008\ K^{-1}$, and $0.0093\ \pm 0.0002\ K^{-1}$. These β values are notably lower than those for hydrocarbon-based polymers, which typically range from 0.016–0.019 K^{-1}.[64] In fact, values in this study are more reminiscent of perfluoropolymers,[63] but the non-fluorinated structure suggests that another material property is influencing these results. When considering S_{inf} values, it should be noted from **Equation 6** that these values are primarily influenced by Langmuir contributions. For example, the Langmuir contribution at infinite dilution, $C'_{\mathrm{H}}b$, represents 98% of the value of S_{inf} for CO_2 at 35 °C for PIM-NH_2. Thus, the weaker dependence of S_{inf} on T_c is likely related to the large excess free volume in these PIM materials relative to traditional polymers that have less excess free volume. Nevertheless, CO_2–amine interaction are still strong in these PIM materials, as noted by the high sorption coefficients. Less condensable gases showed similar S_{inf} values for amine-functionalized and nitrile-functionalized samples, but CO_2 showed a significant boost in S_{inf} for amine-functionalized samples, resulting in steeper β values when considering sorption trends holistically among multiple gases.[60]

The S_{inf} trends presented in **Figure 3c** were further investigated by plotting their Henry and Langmuir contributions (k_{D} and b) against T_c, as shown in **Figures 3d and S15**. The Henry's constant is associated with solubility into the polymer matrix, which necessitates the opening of "gaps" inside the polymer chains. As shown in **Figure 3d**, the trends of k_{D} with T_c remain relatively constant for the two polymer backbones regardless of backbone functionality. This result suggests that the Henry's mode of sorption is more directly influenced by the backbone of the polymer and less affected by the interactions of the penetrant with –NH_2 or –CN

functionality. Similar to the overall S_{inf} versus T_{c} trends, we note that k_{D} versus T_{c} has similar slopes for all samples considered. Thus, the high excess free volume appears to be influencing both the Langmuir and Henry's mode for sorption, resulting in solubility trends with respect to T_{c} for S_{inf} and for the dual-mode parameters that are outside of the traditional trends observed for classic hydrocarbon-based polymers.

We also note that these functional microporous polymers have extraordinary Langmuir-mode contributions, especially in the limit of infinite dilution, and these trends are magnified with increasing FFV. **Figure S15** shows that b, which represents a surface-like sorption–desorption rate between the polymer matrix and the penetrant, generally increases for more condensable gases and, in the case of PIM-NH_2 and PAE-NH_2, increases much more strongly for CO_2 than H_2S. Conversely, b is relatively similar for the less polarizable gases across all materials. This result further suggests strong site-specific interactions with the amines and acid gases despite the lower overall free volume. Lastly, the increase in b when comparing nitrile- to amine-functional polymers is more pronounced in the PIM materials, likely due to higher overall free volume available for Langmuir sorption.

In addition to b, Langmuir capacity (C'_{H}) was also analyzed to more fully understand the effects of amine functionalization and packing structure densification on Langmuir-mode sorption. **Figure S15a** illustrates trends of C'_{H} with FFV for all gases for both PIMs and PAEs. The PIM analogues, which have higher FFV, show a clear positive correlation for C'_{H} as a function of FFV for the less condensable penetrants, N_2 and CH_4. The PAEs, on the other hand, with less non-equilibrium free volume, show relatively constant C'_{H} for N_2 and CH_4, regardless of FFV. Interestingly, the trends are reversed for CO_2 and H_2S, where increasing free volume does not contribute directly to increased Langmuir capacity. Stated another way, adding a primary

amine increases the Langmuir characteristics of microporous polymers, even though FFV is decreased. Taken together, the Langmuir mode strongly contributes to the trends observed for S_{inf} with T_c and thus, to overall sorption in amine-functionalized microporous polymers. The important role of the Langmuir mode to sorption also provides a potential explanation for the higher increase in mixed-gas versus pure-gas permselectivities observed in for PIM-NH_2 compared to PAE-NH_2, which was reported in our corresponding study that focuses on the separation performance of the materials in this work.[65] These findings suggest that, in addition to the –NH_2 functional group, the Langmuir contribution (and therefore polymer FFV) should be maximized to optimize competitive sorption effects.

The particularly high affinities for CO_2 in amine-functionalized polymers are illustrated by plotting these data on the Lipscomb sorption upper bound presented in **Figure S20**.[66] Several unique fundamental insights can be gleaned about the role of amines on gas–polymer partitioning from this analysis. Compared to other microporous polymers, amine-functionalized backbones (PIM-NH_2, PAE-NH_2, PIM-deBOC(acid)[45], and PIM-deBOC(thermal)[45]) have consistently higher CO_2-based S_{inf} values and higher CO_2/CH_4 sorption selectivities at infinite dilution. Notably, PAE-NH_2 and PIM-NH_2 show a significant increase in sorption-based selectivity at infinite dilution (by 108% and 335%, respectively) compared to their nitrile analogues. The increase in sorption-based selectivity for the PIM-based materials in this study is higher than that reported in our previous work.[15] Differences in free volume influenced by solvent pretreatment might explain this discrepancy. However, a non-methanol treated sample of PIM-NH_2 in this study not only surpasses the sorption selectivity of our previous study but also the theoretically derived limit for the sorption upper bound. This interesting result suggests that amine-functional polymers and CO_2–amine interactions may be poorly described using

traditional lattice-based statistical thermodynamic models, such as the non-equilibrium lattice fluid model (NELF), which is the basis for the sorption upper bound. In short, the NELF model relies on a well-known geometric mean assumption to account for CO_2–polymer interactions, but such an assumption ignores atomistic differences in lattice dimensions and interaction energies between CO_2-filled lattices and polymer-segment-filled lattices. From this perspective, amine-functional PIMs are unique. They have among the highest known CO_2 heats of sorption for polymers, which will be described later, approaching energetic behavior more characteristic of hydrogen bonding, and additionally, PIMs are microporous materials. Hence, their microporosity results in pseudo-equilibrium free volume architecture. This interesting finding requires additional theoretical analysis, including the need to calculate cohesive energy density of amine-functional PIMs, and the development of atomistic models and spectroscopic techniques to evaluate possible clustering of functionality and free volume, especially for *in situ* CO_2-based studies. While this analysis is outside the scope of the present study, our findings suggest that amine-functional PIMs provide an extraordinary benefit to competitive sorption for membrane applications, so understanding the underlying mechanism and theory behind this behavior should be a focus within the research community.

3.3.3. Mixed-gas sorption predictions for ternary mixtures

Pure-gas DMS model parameters were used to model the effects of competitive sorption on mixed-gas transport for a 20/20/60 $H_2S/CO_2/CH_4$ ternary mixture. Mixed-gas H_2S, CO_2, and CH_4 sorption isotherms, which were calculated from pure-gas DMS fitting parameters according to **Equation 3**, are shown in **Figure 4a and S16**. This ternary mixture is identical to the experimental ternary permeation tests discussed earlier. In previous DMS modeling work, our group and others have demonstrated how CO_2 mixed-gas sorption is typically unaffected by the

presence of CH_4, while CH_4 mixed-gas sorption significantly decreases as it is excluded from the polymer matrix.[39,40] In the present scenario, H_2S represents a much more condensable penetrant than CO_2, so both CO_2 and CH_4 sorption should decrease significantly while H_2S sorption should remain less affected. These trends have been previously highlighted in DMS modelling by Yi et al.[67] for AO-PIM-1 and PIM-1 in 20/20/60 $H_2S/CO_2/CH_4$ ternary mixtures. Specifically, the relative decreases in predicted sorption for each gas obtained for PIM-1 in the study by Yi et al. are similar to those of this work. As shown in **Figure 4a and S16**, the mixed-gas sorption of all three penetrants in the mixture decreases when in the presence of the other two penetrants. However, when compared to the amine-functionalized samples, the decrease in H_2S mixed-gas sorption for PIM-1 and PAE-CN was notably smaller than that observed for the amine-functionalized samples, suggesting stronger moiety-specific CO_2 interactions from the $-NH_2$ group that result in competition between CO_2 and H_2S for sorption.

Figure 4. (a) H_2S, CO_2 and CH_4 experimental pure-gas isotherms (lines) and modeled mixed-gas sorption isotherms (dashed and dotted lines) for a 20/20/60 $H_2S/CO_2/CH_4$ mixture. (b) Pure-gas CO_2/CH_4 (orange bars) and H_2S/CH_4 (purple bars) sorption selectivities and modeled mixed-gas

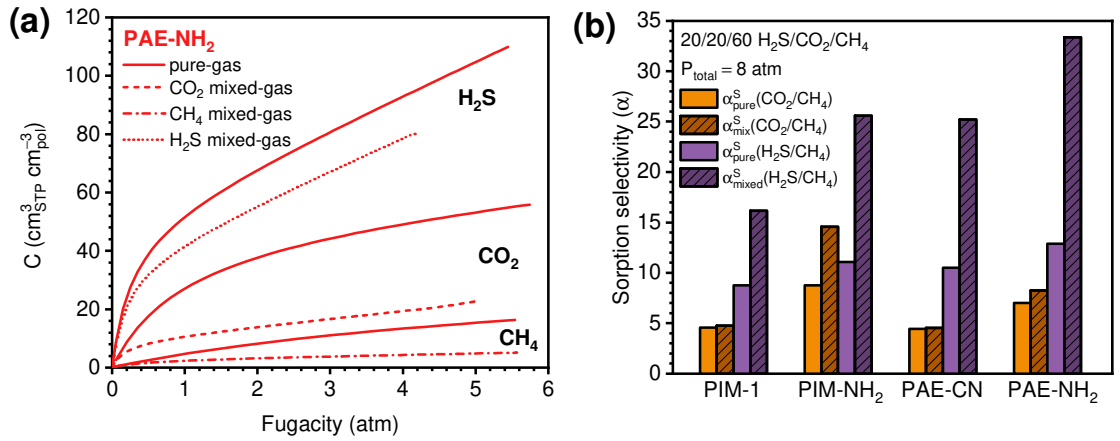

514 CO_2/CH_4 (dark brown and patterned bars) and H_2S/CH_4 (dark purple and patterned bars) sorption
515 selectivities for PIM-1, PIM-NH_2, PAE-CN, and PAE-NH_2.

516 Pure- and mixed-gas CO_2/CH_4 and H_2S/CH_4 sorption selectivities are presented in
517 **Figure 4b**. In all cases, H_2S/CH_4 mixed-gas sorption selectivity increases by more than double
518 that of the pure-gas cases, and the effect is slightly more prominent for PIM-NH_2 and PAE-NH_2.
519 These trends align with the expected competitive effects for a highly condensable penetrant and
520 can positively influence transport performance for the polymer in the absence of competing
521 plasticization effects. On the other hand, mixed-gas CO_2/CH_4 sorption selectivity remains
522 identical to that in the pure-gas case for PIM-1 and PAE-CN while PIM-NH_2 and PAE-NH_2
523 mixed-gas CO_2/CH_4 sorption selectivities still increase compared to the pure-gas case. We
524 finally note that the concentration of H_2S in these test cases represent some of the highest
525 concentrations of H_2S that are found for realistic acid-gas separations.[68] Despite such high
526 concentrations of H_2S, it is remarkable that amine-functional PIMs and PAEs still achieve
527 improvements in mixed-gas performance compared to expectations from pure-gas
528 measurements.[65]

529 **3.3.4. Sorption energetics and isosteric heats of sorption**

530 Sorption energetics were investigated by calculating heats of sorption at infinite dilution
531 ($\Delta H_{S_{inf}}$) for each polymer–gas pair. Analogous to **Equation 7**, $\Delta H_{S_{inf}}$ can be calculated from
532 trends of S_{inf} for variable temperatures according to **Equation 11**:

533 $$S_{inf} = S_{inf,0} \exp\left(-\frac{\Delta H_{S_{inf}}}{RT}\right) \quad (11)$$

where $S_{\mathrm{inf},0}$ is a pre-exponential factor embedding the entropic terms associated with infinite dilution sorption ($cm^3_{STP}\ cm^{-3}_{pol}\ atm^{-1}$). As shown in **Equations 8 and 9**, Henry's and Langmuir mode contributions to sorption follow similar van't Hoff relationships with temperature, where ΔH_{D} and ΔH_{b} represent the energy difference between the penetrant in the gaseous state, H_{g}, and the penetrant sorbed in its respective mode (i.e., $\Delta H_{\mathrm{D}\ or\ \mathrm{b}} = H_{\mathrm{D}\ or\ \mathrm{b}} - H_{\mathrm{g}}$).[69]

The $\Delta H_{S_{\mathrm{inf}}}$ values for each gas–polymer pair are presented in **Figure 5 and Table S8**. The values of $\Delta H_{S_{\mathrm{inf}}}$ ranged from –16 kJ mol^{-1} for N_2 to –38 kJ mol^{-1} for CO_2, respectively. These values are consistent with general trends observed for hydrocarbon-based polymers.[21] Moreover, $\Delta H_{S_{\mathrm{inf}}}$ values in PIM-1 align well with previously reported values for N_2 (–14 kJ mol^{-1}), CH_4 (–19 kJ mol^{-1}) and CO_2 (–22 kJ mol^{-1}).[43] To the best of our knowledge, there are no reported H_2S sorption isotherms at variable temperatures for PIM-1 or for the three other polymers considered. Generally, $\Delta H_{S_{\mathrm{inf}}}$ values represent the thermodynamic favorability associated with mixing of the gas penetrant with the polymer matrix. In typical hydrocarbon-based polymers, the more condensable gases will more favorably partition into the polymer matrix, resulting in more exothermic sorption interactions. These trends are directly observed for PIM-1 and PAE-CN.

In contrast, the amine-functional samples exhibited unique sorption behavior. Analogous to the CO_2-specific trends observed for S_{inf} and k_D, PIM-NH_2 and PAE-NH_2 have significantly higher $\Delta H_{S_{inf}}$ values for CO_2 than for H_2S, which is attributed to the CO_2-specific interactions with the –NH_2 moiety. **Figure S17** summarizes the contributions of ΔH_D and ΔH_b for each gas–polymer pair, where the trends for ΔH_b mirror those reviewed earlier for $\Delta H_{S_{inf}}$. Sorption energetic trends for the Henry's law mode of sorption remain relatively constant across

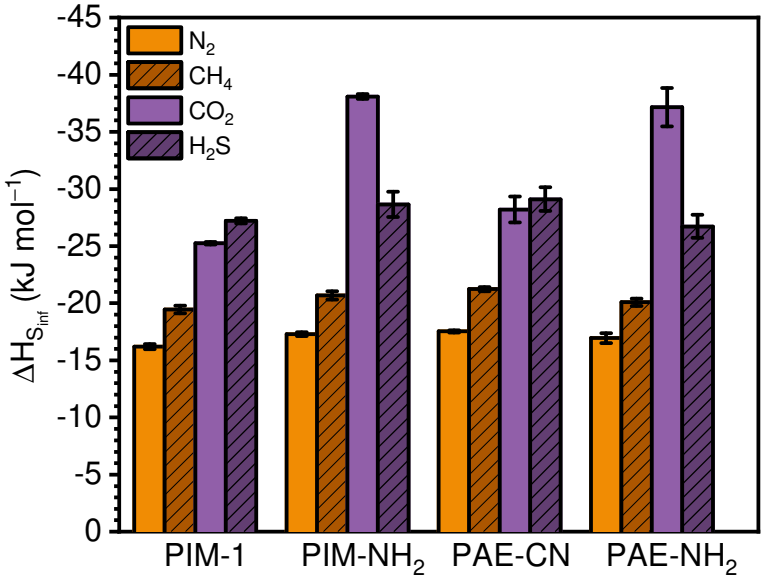

gases, with some deviations observed for N_2 in PIM-1 and CO_2 in PIM-NH_2.

Figure 5. N_2, CH_4, CO_2 and H_2S $\Delta H_{S_{inf}}$values calculated for PIM-1, PIM-NH_2, PAE-CN, and PAE-NH_2. Error bars were determined from error propagation of the slope and intercept errors on the log-transformed version of **Equation 11**, provided by Microsoft Excel's LINEST function.

562 Isosteric heats were calculated to investigate CH_4, CO_2, and H_2S sorption energetics
563 across penetrant composition for the gas–polymer pairs considered, as shown in **Figure 6 and**
564 **Figure S18**. N_2 curves have subtle differences that are largely within error of each other, thus,
565 the more condensable gases were taken as the primary focus of this discussion. CH_4, CO_2 and
566 H_2S isosteric heats all show minima at lower concentrations in PAEs than in PIMs. In the context
567 of the dual-mode model, the minimum of an isosteric heat curve generally represents a transition
568 from the Langmuir regime to less favorable enthalpic interactions in the Henry's law mode. This
569 transition occurs earlier for PAEs due to their denser packing structure, which correlates directly
570 with their lower FFV. In other words, PAEs reach their Langmuir capacity at a lower
571 concentration of gas sorption than PIMs. The largest differences between the isosteric heat
572 curves were observed between nitrile- and amine-functionalized samples for CO_2. Interestingly,
573 PIM-NH_2 and PAE-NH_2 show remarkably exothermic minima of –44 kJ mol^{-1}. These highly
574 favorable exothermic interactions between CO_2 and the –NH_2 surpass the minima observed for
575 isosteric heats of H_2S, which are between –34 kJ mol^{-1} and –31 kJ mol^{-1} for PIM-NH_2 and PAE-
576 NH_2, respectively. Moreover, H_2S isosteric heats remain largely within error of each other

between polymers with the same backbone, while CO_2 isosteric heats for PIM-NH_2 and PAE-NH_2 show significant differences in exothermicity.

Figure 6. (a) CO_2 and (b) H_2S isosteric heats of sorption for PIM-1, PIM-NH_2, PAE-CN, and PAE-NH_2. Error bars are represented by light lines with the area of the error shaded in the corresponding color. Dashed lines indicate equimolar CO_2 or H_2S concentrations that correspond with respect to amine groups in each polymer.

There are various physical and chemical interactions that can occur between CO_2 and primary amines. These interactions become increasingly complex with amines that are close neighbors, which can introduce cooperative interactions, and for amines in humid environments.[70] For amine-functionalized solids in dry conditions, CO_2 capture at its highest efficiency occurs at a 2:1 ratio of $-NH_2$ to CO_2 through the formation of a carbamate.[71] However, the O'Brien group has recently investigated the transport mechanism for CO_2 in polyvinylamine (PVAm) membranes using an in situ spectroscopic apparatus, and their results show that

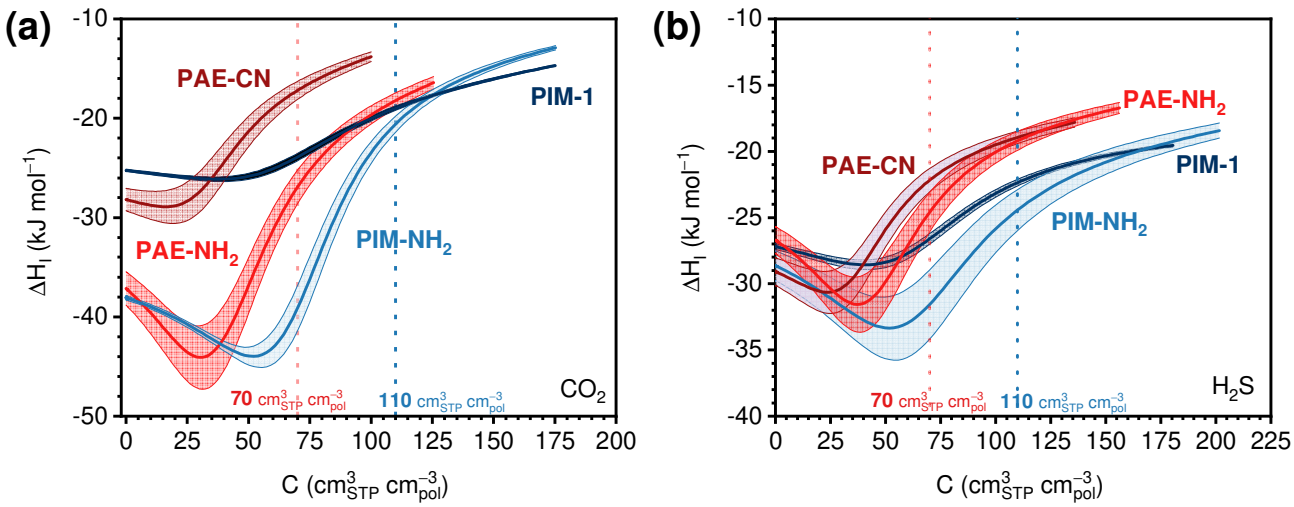

carbamate formation only occurs in humid conditions.[72,73] Nevertheless, it remains of interest to investigate the mechanism of CO_2 transport in other primary-amine-functional polymers, such as

the microporous materials in this study. Specifically, the reaction in question between CO_2 and the primary amine in dry conditions is described by **Equations 12 and 13** below[74–76]:

$$CO_2 + RNH_2 \rightarrow RNH_2{}^+COO^- \quad (12)$$

$$RNH_2{}^+COO^- + RNH_2 \rightarrow RNH_3{}^+ + RNHCOO^- \quad (13)$$

As described in the equations above, after an initial reaction between a primary amine and CO_2 to form an $–H_2N^+COO^–$ zwitterion, a second amine in proximity to the zwitterion can accept a proton from the zwitterion, thus requiring 2 $–NH_2$ moieties for every CO_2 sorbed. Because this mechanism requires amines to be situated close to one another, it has been shown that high amine loading facilitates this reaction.[77] Additionally, H_2S is also believed to interact with the primary amine group in the same ratio as does CO_2. This physical interaction is shown below[78]:

$$H_2S + 2\,RNH_2 \rightarrow RH_2N \cdots HSH \cdots NH_2R \quad (14)$$

Equation 14 describes the formation of an H_2S–amine complex, where the hydrogen atoms on H_2S hydrogen-bond to the nitrogen atoms on two neighboring amine groups.[79–81] This complex is illustrated in **Figure 7**. The heat of adsorption for this process has been reported to be in the range of −24 to −33 kJ mol^{-1} for silica-supported amine sorbents,[79] values that are well within the range of those found for PIM-NH_2 and PAE-NH_2 in this work.

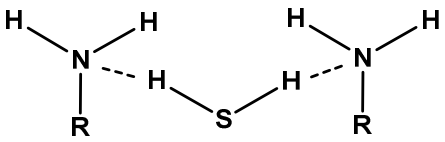

Figure 7. H_2S–amine complex that is believed to form in dry conditions.[79–81]

In the context of isosteric heats of sorption and the dual-mode model, the minima observed in **Figure 6** can be understood as the transition from the Langmuir to the Henry's mode after statistical partitioning into the Langmuir mode becomes less favorable. Interestingly, the molar concentration of $–NH_2$ groups in the polymer backbone is approximately twice the concentration of CO_2 and H_2S at these minima. These results are highlighted in **Figure 6**, and they could be used to support an interpretation of (1) chemisorption in the case of CO_2 and (2) the formation of an H_2S–amine complex in the case of H_2S. However, a few more points need to be considered. First, we considered if the apparent 2:1 N:CO_2 and N:H_2S ratios are unique to the amine-functional materials as opposed to the nitrile-functional polymers, where the mechanisms described above should not apply. A summary of the concentration ratios for all four materials can be found in **Table 1**.

Table 1. N:CO_2 and N:H_2S concentration ratios observed at the CO_2 and H_2S isosteric heat minima, respectively, for PIM-1, PIM-NH_2, PAE-CN, and PAE-NH_2.

Material	Nitrogen molar concentration (cm^3_{STP} cm^{-3}_{pol})	CO_2 concentration at isosteric heat minimum (cm^3_{STP} cm^{-3}_{pol})	H_2S concentration at isosteric heat minimum (cm^3_{STP} cm^{-3}_{pol})	N:CO_2 ratio at isosteric heat minimum	N:H_2S at isosteric heat minimum
PIM-1	111	38.0	40.9	2.9	2.7
PIM-NH_2	110	52.1	51.7	2.1	2.1
PAE-CN	69.0	16.0	24.2	4.3	2.9
PAE-NH_2	70.2	30.0	37.0	2.3	1.9

For PAE-CN and PIM-1, the nitrogen molar concentrations in the polymers are 4.3 and 2.9 times higher the concentrations of CO_2 at the isosteric heat minima, respectively. These

values, which are larger than the theoretical 2:1 ratio, show that the interaction between –CN and CO_2 does not follow the pathway described in **Equations 12 and 13**, confirming that CO_2 sorption in these nitrile-functional materials is most likely described by physisorption rather than chemisorption. Regarding sorption of H_2S, the nitrogen molar concentrations in the amine-functional polymers also lie at approximately double the concentrations of H_2S at the observed isosteric heat minima. The nitrile-functional PAE-CN and PIM-1, on the other hand, exhibit N:H_2S ratios of 2.9 and 2.7, respectively. The 2:1 –NH_2:CO_2 and –NH_2:H_2S ratios found for both PIM-NH_2 and PAE-NH_2 indicate that CO_2 and H_2S sorption in these materials is potentially driven by known mechanisms described in the equations above,[71,78] whereas the analogous N:CO_2 and N:H_2S ratios found for the nitrile-functional PIM-1 and PAE-CN indicate that sorption in these materials is likely driven by ordinary physisorption. However, these ratios could simply be coincidental. Direct in situ spectroscopy experiments, such as those by the O'Brien group,[72,73] would be essential for evaluating reaction species and intermediate complexes. Additionally, the amine molar concentrations in PAE-NH_2 and PIM-NH_2 are likely too low to allow for the carbamate-forming mechanism described earlier. Given the rigid backbones of the polymers considered in this study coupled with amine groups that make up only 3% and 5% by volume of PAE-NH_2 and PIM-NH_2, respectively, short range ordering and –NH_2 cluster formation is unlikely. These small volume fractions, which we calculated using the reported van der Waals volumes from the Wu group contribution method,[57] indicate that the probability that two amine groups are neighboring each other is less than 0.3% at most, assuming a random statistical distribution.

4. Conclusions

A new amine-functionalized microporous polymer (PAE-NH_2) based on spirobifluorene and triptycene structural units was synthesized from a nitrile-functionalized poly(arylene ether) (PAE-CN). Chemical characterization showed successful functionalization of the PAE-CN to PAE-NH_2. The effects of amine-functionalization on the polymer packing structure as well as CO_2- and H_2S-specific transport behavior were investigated through FFV calculations and mixed-gas sorption predictions. Findings for the PAE samples were directly compared to PIM-1 and its amine-functionalized analogue, PIM-NH_2, through additional testing and characterization. Gas–polymer interactions were probed through N_2, CH_4, CO_2, and H_2S pure-gas sorption tests at 35 °C, 45 °C, 55 °C, and 65 °C and the data was interpreted via the dual-mode model framework. Compared to all other gases including H_2S, CO_2 sorption in PAE-NH_2 and PIM-NH_2 was noticeably higher than that in PAE-CN and PIM-1, respectively, suggesting that increases in mixed-gas performance for CO_2- and H_2S-based separations that were observed in our complementary study on mixed-gas transport[65] are driven by sorption. For PAE-NH_2 and PIM-NH_2, sorption at infinite dilution for CO_2 was particularly high relative to other microporous polymers. The strength of the CO_2–polymer interactions was quantified through calculations of isosteric heats of sorption for CO_2 in PIM-1, PIM-NH_2, PAE-CN, and PAE-NH_2. Amine-functionalized samples showed significantly more exothermic interactions with CO_2 compared to the nitrile-functionalized analogues, suggesting moiety specific interactions. The results of this work, taken together with the competition-enhanced separation performance reported in our permeation-focused study of the same materials,[65] demonstrate that addition of primary amines to microporous polymers can be leveraged to enhance mixed-gas performance through competition, especially for CO_2-based separations.

CRediT author statement

Pablo A. Dean and **Katherine Mizrahi Rodriguez:** Conceptualization, Methodology, Investigation, Formal Analysis, Data Curation, Writing – Original Draft. **Sheng Guo**: Investigation, Writing – Review and Editing. **Naksha Roy**: Investigation, Formal Analysis, Writing – Review and Editing. **Timothy M. Swager**: Conceptualization, Writing – Review and Editing. **Zachary P. Smith:** Conceptualization, Writing – Review and Editing, Supervision.

Declaration of competing interest

The authors have no known competing financial interests or personal relationships that could influence the work reported in this paper.

Acknowledgements

This work was supported by the U.S. Department of Energy, Office of Science, Office of Basic Energy Sciences, Separation Science program (award number: DE-SC0019087). We also gratefully acknowledge the Department of Navy, Office of Naval Research under ONR awards N00014-20-1-2418 and N00014-21-1-2666 for support in the development and testing of novel microporous polymers and for support in elucidating the role of competitive sorption in membrane materials. Additionally, we are grateful to Eni S.p.A. for support through the MIT Energy Initiative in polymer development for H_2S-based separations. Pablo A. Dean acknowledges support from an NSF-GRFP fellowship (DGE-2141064). K. Mizrahi Rodriguez acknowledges support from an NSF-GRFP fellowship (DGE-1122374). This study made use of the shared facilities available at MIT, including the Materials Research Laboratory and the Department of Chemistry Instrumentation Facility. The authors gratefully acknowledge input from Albert X. Wu on sorption analysis and dual-mode modeling, as well as Walter Maseffski, John Grimes, and Bruce Adams for help with NMR analysis.

6. References

(1) Demirbaş, A. Combustion Properties and Calculation Higher Heating Values of Diesel Fuels. *Pet. Sci. Technol.* **1998**, *16* (7–8). https://doi.org/10.1080/10916469808949811.

(2) R. C. Assunção, L.; A. S. Mendes, P.; Matos, S.; Borschiver, S. Technology Roadmap of Renewable Natural Gas: Identifying Trends for Research and Development to Improve Biogas Upgrading Technology Management. *Appl. Energy* **2021**, *292*, 116849. https://doi.org/10.1016/j.apenergy.2021.116849.

(3) Alcheikhhamdon, Y.; Hoorfar, M. Natural Gas Purification from Acid Gases Using Membranes: A Review of the History, Features, Techno-Commercial Challenges, and Process Intensification of Commercial Membranes. *Chem. Eng. and Processing: Process Intensification*. 2017, pp 105–113. https://doi.org/10.1016/j.cep.2017.07.009.

(4) Alkatheri, M.; Grandas, R.; Betancourt-Torcat, A.; Almansoori, A. Tapping Singular Middle Eastern Ultrasour Gas Resources Combining Membrane and Absorption Systems: Potential for Energy Intensity Reduction. *Ind. Eng. Chem. Res.* **2018**, *57* (17), 5748–5763. https://doi.org/10.1021/acs.iecr.7b02200.

(5) Harrigan, D. J.; Lawrence, J. A.; Reid, H. W.; Rivers, J. B.; O'Brien, J. T.; Sharber, S. A.; Sundell, B. J. Tunable Sour Gas Separations: Simultaneous H_2S and CO_2 Removal from Natural Gas via Crosslinked Telechelic Poly(Ethylene Glycol) Membranes. *J. Membr. Sci.* **2020**, *602*, 117947. https://doi.org/10.1016/j.memsci.2020.117947.

(6) Baker, R. W.; Lokhandwala, K. Natural Gas Processing with Membranes: An Overview. *Ind. Eng. Chem. Res*. American Chemical Society April 2, 2008, pp 2109–2121. https://doi.org/10.1021/ie071083w.

(7) Yi, S.; Ghanem, B.; Liu, Y.; Pinnau, I.; Koros, W. J. Ultraselective Glassy Polymer Membranes with Unprecedented Performance for Energy-Efficient Sour Gas Separation. *Sci. Adv.* **2019**, *5* (5), eaaw5459. https://doi.org/10.1126/sciadv.aaw5459.

(8) Yi, S.; Ma, X.; Pinnau, I.; Koros, W. J. A High-Performance Hydroxyl-Functionalized Polymer of Intrinsic Microporosity for an Environmentally Attractive Membrane-Based Approach to Decontamination of Sour Natural Gas. *J. Mater. Chem. A* **2015**, *3* (45), 22794–22806. https://doi.org/10.1039/c5ta05928c.

(9) Sholl, D. S.; Lively, R. P. Seven Chemical Separations to Change the World. *Nature* **2016**, *532* (7600), 435–437. https://doi.org/10.1038/532435a.

(10) Sholl, D. S.; Lively, R. P. Exemplar Mixtures for Studying Complex Mixture Effects in Practical Chemical Separations. *JACS Au* **2022**. https://doi.org/10.1021/jacsau.1c00490.

(11) Vopička, O.; De Angelis, M. G.; Sarti, G. C. Mixed Gas Sorption in Glassy Polymeric Membranes: I. CO_2/CH_4 and n-C_4/CH_4 Mixtures Sorption in Poly(1-Trimethylsilyl-1-Propyne) (PTMSP). *J. Membr. Sci.* **2014**, *449*, 97–108. https://doi.org/10.1016/j.memsci.2013.06.065.

(12) Vopička, O.; De Angelis, M. G.; Du, N.; Li, N.; Guiver, M. D.; Sarti, G. C. Mixed Gas Sorption in Glassy Polymeric Membranes: II. CO_2/CH_4 Mixtures in a Polymer of Intrinsic Microporosity (PIM-1). *J. Membr. Sci.* **2014**, *459*, 264–276. https://doi.org/10.1016/j.memsci.2014.02.003.

(13) Sanders, E. S.; Koros, W. J.; Hopfenberg, H. B.; Stannett, V. T. Mixed Gas Sorption in Glassy Polymers: Equipment Design Considerations and Preliminary Results. *J. Membr. Sci.* **1983**, *13* (2), 161–174. https://doi.org/10.1016/S0376-7388(00)80159-3.

(14) Ricci, E.; Benedetti, F. M.; Noto, A.; Merkel, T. C.; Jin, J.; De Angelis, M. G. Enabling Experimental Characterization and Prediction of Ternary Mixed-Gas Sorption in Polymers: $C_2H_6/CO_2/CH_4$ in PIM-1. *Chem. Eng. Journ.* **2021**, *426*, 130715. https://doi.org/10.1016/j.cej.2021.130715.

(15) Mizrahi Rodriguez, K.; Benedetti, F. M.; Roy, N.; Wu, A. X.; Smith, Z. P. Sorption-Enhanced Mixed-Gas Transport in Amine Functionalized Polymers of Intrinsic Microporosity (PIMs). *J. Mater. Chem. A* **2021**, *9* (41), 23631–23642. https://doi.org/10.1039/d1ta06530k.

(16) Wang, Y.; Ma, X.; Ghanem, B. S.; Alghunaimi, F.; Pinnau, I.; Han, Y. Polymers of Intrinsic Microporosity for Energy-Intensive Membrane-Based Gas Separations. *Mater. Today. Nano.* **2018**, *3* (2018), 69–95. https://doi.org/10.1016/j.mtnano.2018.11.003.

(17) Sanders, D. F.; Smith, Z. P.; Guo, R.; Robeson, L. M.; McGrath, J. E.; Paul, D. R.; Freeman, B. D. Energy-Efficient Polymeric Gas Separation Membranes for a Sustainable Future: A Review. *Polymer*. 2013. https://doi.org/10.1016/j.polymer.2013.05.075.

(18) Suleman, M. S.; Lau, K. K.; Yeong, Y. F. Plasticization and Swelling in Polymeric Membranes in CO_2 Removal from Natural Gas. *Chem. Eng. Technol*. 2016. https://doi.org/10.1002/ceat.201500495.

(19) Bos, A.; Pünt, I. G. M.; Wessling, M.; Strathmann, H. Suppression of CO_2-Plasticization by Semiinterpenetrating Polymer Network Formation. *J. Polym. Sci. B Polym. Phys.* **1998**, *36* (9). https://doi.org/10.1002/(SICI)1099-0488(19980715)36:9<1547::AID-POLB12>3.0.CO;2-5.

(20) Koros, W. J.; Chern, R. T.; Stannett, V.; Hopfenberg, H. B. Model for Permeation of Mixed Gases and Vapors in Glassy Polymers. *J. polym. sci. Part A-2, Polym. Phys.* **1981**, *19* (10), 1513–1530. https://doi.org/10.1002/pol.1981.180191004.

(21) Wu, A. X.; Drayton, J. A.; Mizrahi Rodriguez, K.; Benedetti, F. M.; Qian, Q.; Lin, S.; Smith, Z. P. Elucidating the Role of Fluorine Content on Gas Sorption Properties of Fluorinated Polyimides. *Macromolecules* **2021**, *54* (1), 22–34. https://doi.org/10.1021/acs.macromol.0c01746.

(22) Chatterjee, G.; Houde, A. A.; Stern, S. A. Poly(Ether Urethane) and Poly(Ether Urethane Urea) Membranes with High H_2S/CH_4 Selectivity. *J. Membr. Sci.* **1997**, *135* (1), 99–106. https://doi.org/10.1016/S0376-7388(97)00134-8.

(23) Merkel, T. C.; Gupta, R. P.; Turk, B. S.; Freeman, B. D. Mixed-Gas Permeation of Syngas Components in Poly(Dimethylsiloxane) and Poly(1-Trimethylsilyl-1-Propyne) at Elevated Temperatures. *J. Membr. Sci.* **2001**, *191* (1–2). https://doi.org/10.1016/S0376-7388(01)00452-5.

(24) Kraftschik, B.; Koros, W. J. Cross-Linkable Polyimide Membranes for Improved Plasticization Resistance and Permselectivity in Sour Gas Separations. *Macromolecules* **2013**, *46* (17), 6908–6921. https://doi.org/10.1021/ma401542j.

(25) Kraftschik, B.; Koros, W. J.; Johnson, J. R.; Karvan, O. Dense Film Polyimide Membranes for Aggressive Sour Gas Feed Separations. *J. Membr. Sci.* **2013**, *428*, 608–619. https://doi.org/10.1016/j.memsci.2012.10.025.

(26) Vaughn, J.; Koros, W. J. Effect of the Amide Bond Diamine Structure on the CO_2, H_2S, and CH_4 Transport Properties of a Series of Novel 6FDA-Based Polyamide-Imides for Natural Gas Purification. *Macromolecules* **2012**, *45* (17), 7036–7049. https://doi.org/10.1021/ma301249x.

(27) Achoundong, C. S. K.; Bhuwania, N.; Burgess, S. K.; Karvan, O.; Johnson, J. R.; Koros, W. J. Silane Modification of Cellulose Acetate Dense Films as Materials for Acid Gas Removal. *Macromolecules* **2013**, *46* (14), 5584–5594. https://doi.org/10.1021/ma4010583.

(28) Liu, Y.; Liu, Z.; Morisato, A.; Bhuwania, N.; Chinn, D.; Koros, W. J. Natural Gas Sweetening Using a Cellulose Triacetate Hollow Fiber Membrane Illustrating Controlled Plasticization Benefits. *J. Membr. Sci.* **2020**, *601*, 117910. https://doi.org/10.1016/j.memsci.2020.117910.

(29) Harrigan, D. J.; Yang, J.; Sundell, B. J.; Lawrence, J. A.; O'Brien, J. T.; Ostraat, M. L. Sour Gas Transport in Poly(Ether-b-Amide) Membranes for Natural Gas Separations. *J. Membr. Sci.* **2020**, *595*, 117497. https://doi.org/10.1016/j.memsci.2019.117497.

(30) Swaidan, R.; Ghanem, B.; Pinnau, I. Fine-Tuned Intrinsically Ultramicroporous Polymers Redefine the Permeability/Selectivity Upper Bounds of Membrane-Based Air and Hydrogen Separations. *ACS Macro Letters*. American Chemical Society September 15, 2015, pp 947–951. https://doi.org/10.1021/acsmacrolett.5b00512.

(31) Mizrahi Rodriguez, K.; Benedetti, F. M.; Roy, N.; Wu, A. X.; Smith, Z. P. Sorption-Enhanced Mixed-Gas Transport in Amine Functionalized Polymers of Intrinsic Microporosity (PIMs). *J. Mater. Chem. A* **2021**, *9* (41), 23631–23642. https://doi.org/10.1039/d1ta06530k.

(32) Guo, S.; Swager, T. M. Versatile Porous Poly(Arylene Ether)s via Pd-Catalyzed C-O Polycondensation. *J. Am. Chem. Soc.* **2021**, *143* (30), 11828–11835. https://doi.org/10.1021/jacs.1c05853.

(33) Guo, S.; Yeo, J. Y.; Benedetti, F. M.; Syar, D.; Swager, T. M.; Smith, Z. P. A Microporous Poly(Arylene Ether) Platform for Membrane-Based Gas Separation. *Angew. Chem. International Edition* **2023**. https://doi.org/10.1002/anie.202315611.

(34) Wijmans, J. G.; Baker, R. W. The Solution-Diffusion Model: A Review. *J. Membr. Sci.* **1995**, *107* (1–2), 1–21. https://doi.org/10.1016/0376-7388(95)00102-I.

(35) PAUL DR. Effect of Immobilizing Adsorption on the Diffusion Time Lag. *J. Polym. Sci. Part A-2 Polym. Phys.* **1969**, *7* (10), 1811–1818. https://doi.org/10.1002/pol.1969.160071015.

(36) Fredrickson, G. H.; Helfand, E. Dual-Mode Transport of Penetrants in Glassy Polymers. *Macromolecules* **1985**, *18* (11), 2201–2207. https://doi.org/10.1021/ma00153a024.

(37) Ricci, E.; De Angelis, M. G. Modelling Mixed-Gas Sorption in Glassy Polymers for CO_2 Removal: A Sensitivity Analysis of the Dual Mode Sorption Model. *Membranes (Basel)* **2019**, *9* (1), 1–23. https://doi.org/10.3390/membranes9010008.

(38) C., E. L.; Bevington, P. R. Data Reduction and Error Analysis for the Physical Sciences. *J. Am. Stat. Assoc.* **1972**, *67* (337), 249. https://doi.org/10.2307/2284752.

(39) Ricci, E.; Benedetti, F. M.; Dose, M. E.; De Angelis, M. G.; Freeman, B. D.; Paul, D. R. Competitive Sorption in CO_2/CH_4 Separations: The Case of HAB-6FDA Polyimide and Its TR Derivative and a General Analysis of Its Impact on the Selectivity of Glassy Polymers at Multicomponent Conditions. *J. Membr. Sci.* **2020**, *612*, 118374. https://doi.org/10.1016/j.memsci.2020.118374.

(40) Mizrahi Rodriguez, K.; Benedetti, F. M.; Roy, N.; Wu, A. X.; Smith, Z. P. Sorption-Enhanced Mixed-Gas Transport in Amine Functionalized Polymers of Intrinsic Microporosity (PIMs). *J. Mater. Chem. A* **2021**, *9* (41), 23631–23642. https://doi.org/10.1039/d1ta06530k.

(41) Costello, L. M.; Koros, W. J. Temperature Dependence of Gas Sorption and Transport Properties in Polymers: Measurement and Applications. *Ind. Eng. Chem. Res.* **1992**, *31* (12), 2708–2714. https://doi.org/10.1021/ie00012a012.

(42) Koros, W. J.; Paul, D. R.; Huvard, G. S. Energetics of Gas Sorption in Glassy Polymers. *Polymer* **1979**, *20* (8), 956–960. https://doi.org/10.1016/0032-3861(79)90192-7.

(43) Li, P.; Chung, T. S.; Paul, D. R. Temperature Dependence of Gas Sorption and Permeation in PIM-1. *J. Membr. Sci.* **2014**, *450*, 380–388. https://doi.org/10.1016/j.memsci.2013.09.030.

(44) Mason, C. R.; Maynard-Atem, L.; Heard, K. W. J.; Satilmis, B.; Budd, P. M.; Friess, K.; Lancì, M.; Bernardo, P.; Clarizia, G.; Jansen, J. C. Enhancement of CO_2 Affinity in a Polymer of Intrinsic Microporosity by Amine Modification. *Macromolecules* **2014**, *47* (3), 1021–1029. https://doi.org/10.1021/ma401869p.

(45) Mizrahi Rodriguez, K.; Lin, S.; Wu, A. X.; Han, G.; Teesdale, J. J.; Doherty, C. M.; Smith, Z. P. Leveraging Free Volume Manipulation to Improve the Membrane Separation Performance of Amine-Functionalized PIM-1. *Angew. Chem.* **2021**, *133* (12), 6667–6673. https://doi.org/10.1002/ange.202012441.

(46) Song, Q.; Cao, S.; Pritchard, R. H.; Ghalei, B.; Al-Muhtaseb, S. A.; Terentjev, E. M.; Cheetham, A. K.; Sivaniah, E. Controlled Thermal Oxidative Crosslinking of Polymers of Intrinsic Microporosity towards Tunable Molecular Sieve Membranes. *Nat. Commun*. **2014**, *5*, 4813. https://doi.org/10.1038/ncomms5813.

(47) Saufi, S. M.; Ismail, A. F. Fabrication of Carbon Membranes for Gas Separation - A Review. *Carbon N Y* **2004**, *42* (2), 241–259. https://doi.org/10.1016/j.carbon.2003.10.022.

(48) Jue, M. L.; Lively, R. P. PIM Hybrids and Derivatives: How to Make a Good Thing Better. *Curr. Opin. Chem. Eng.* **2022**, *35*, 100750. https://doi.org/10.1016/j.coche.2021.100750.

(49) Corrado, T.; Guo, R. Macromolecular Design Strategies toward Tailoring Free Volume in Glassy Polymers for High Performance Gas Separation Membranes. *Molec. Syst. Des. Eng*. Royal Society of Chemistry January 1, 2020, pp 22–48. https://doi.org/10.1039/c9me00099b.

(50) Weidman, J. R.; Luo, S.; Breier, J. M.; Buckley, P.; Gao, P.; Guo, R. Triptycene-Based Copolyimides with Tailored Backbone Rigidity for Enhanced Gas Transport. *Polymer* **2017**, *126*, 314–323. https://doi.org/10.1016/j.polymer.2017.04.016.

(51) Wiegand, J. R.; Smith, Z. P.; Liu, Q.; Patterson, C. T.; Freeman, B. D.; Guo, R. Synthesis and Characterization of Triptycene-Based Polyimides with Tunable High Fractional Free Volume for Gas Separation Membranes. *J. Mater. Chem. A* **2014**, *2* (33), 13309–13320. https://doi.org/10.1039/c4ta02303j.

(52) Mizrahi Rodriguez, K.; Wu, A. X.; Qian, Q.; Han, G.; Lin, S.; Benedetti, F. M.; Lee, H.; Chi, W. S.; Doherty, C. M.; Smith, Z. P. Facile and Time-Efficient Carboxylic Acid Functionalization of PIM-1: Effect on Molecular Packing and Gas Separation Performance. *Macromolecules* **2020**, *53* (15), 6220–6234. https://doi.org/10.1021/acs.macromol.0c00933.

(53) Maeda, Y.; Paul, D. R. Effect of Antiplasticization on Gas Sorption and Transport. III. Free Volume Interpretation. *J. Polym. Sci. B Polym. Phys.* **1987**, *25* (5). https://doi.org/10.1002/polb.1987.090250503.

(54) Thran, A.; Kroll, C.; Faupel, F. Correlation between Fractional Free Volume and Diffusivity of Gas Molecules in Glassy Polymers. *J. Polym. Sci. B Polym. Phys.* **1999**, *37* (23). https://doi.org/10.1002/(SICI)1099-0488(19991201)37:23<3344::AID-POLB10>3.0.CO;2-A.

(55) Weber, J.; Meng, Q. B. Microporous Polymers: Synthesis, Characterization, and Applications. In *Encycl. Polym. Sci. Technol.*; 2014. https://doi.org/10.1002/0471440264.pst622.

(56) Hart, K. E.; Abbott, L. J.; Colina, C. M. Analysis of Force Fields and BET Theory for Polymers of Intrinsic Microporosity. *Mol. Simul.* **2013**, *39* (5). https://doi.org/10.1080/08927022.2012.733945.

(57) Wu, A. X.; Lin, S.; Mizrahi Rodriguez, K.; Benedetti, F. M.; Joo, T.; Grosz, A. F.; Storme, K. R.; Roy, N.; Syar, D.; Smith, Z. P. Revisiting Group Contribution Theory for Estimating Fractional Free Volume of Microporous Polymer Membranes. *J. Membr. Sci.* **2021**, *636*. https://doi.org/10.1016/j.memsci.2021.119526.

(58) Vopička, O.; Friess, K.; Hynek, V.; Sysel, P.; Zgažar, M.; Šípek, M.; Pilnáček, K.; Lanč, M.; Jansen, J. C.; Mason, C. R.; Budd, P. M. Equilibrium and Transient Sorption of Vapours and Gases in the Polymer of Intrinsic Microporosity PIM-1. *J. Membr. Sci.* **2013**, *434*, 148–160. https://doi.org/10.1016/j.memsci.2013.01.040.

(59) Park, J. Y.; Paul, D. R. Correlation and Prediction of Gas Permeability in Glassy Polymer Membrane Materials via a Modified Free Volume Based Group Contribution Method. *J. Membr. Sci.* **1997**, *125* (1), 23–39. https://doi.org/10.1016/S0376-7388(96)00061-0.

(60) McDermott, A. G.; Larsen, G. S.; Budd, P. M.; Colina, C. M.; Runt, J. Structural Characterization of a Polymer of Intrinsic Microporosity: X-Ray Scattering with Interpretation Enhanced by Molecular Dynamics Simulations. *Macromolecules* **2011**, *44* (1), 14–16. https://doi.org/10.1021/ma1024945.

(61) Bezzu, C. G.; Carta, M.; Ferrari, M. C.; Jansen, J. C.; Monteleone, M.; Esposito, E.; Fuoco, A.; Hart, K.; Liyana-Arachchi, T. P.; Colina, C. M.; McKeown, N. B. The Synthesis, Chain-Packing Simulation and Long-Term Gas Permeability of Highly Selective Spirobifluorene-Based Polymers of Intrinsic Microporosity. *J. Mater. Chem. A* **2018**, *6* (22), 10507–10514. https://doi.org/10.1039/c8ta02601g.

(62) Li, P.; Chung, T. S.; Paul, D. R. Gas Sorption and Permeation in PIM-1. *J. Membr. Sci.* **2013**, *432*, 50–57. https://doi.org/10.1016/j.memsci.2013.01.009.

(63) Smith, Z. P.; Tiwari, R. R.; Dose, M. E.; Gleason, K. L.; Murphy, T. M.; Sanders, D. F.; Gunawan, G.; Robeson, L. M.; Paul, D. R.; Freeman, B. D. Influence of Diffusivity and Sorption on Helium and Hydrogen Separations in Hydrocarbon, Silicon, and Fluorocarbon-Based Polymers. *Macromolecules* **2014,** *47* (9), 3170-3184. https://doi.org/10.1021/ma402521h.

(64) Yampolskii, Y.; Pinnau, I.; Freeman, B. D. *Mater. Sci. Membr. Gas Vap. Sep.*; Yampolskii, Y., Pinnau, I., Freeman, B., Eds.; John Wiley & Sons, Ltd: Chichester, UK, 2006. https://doi.org/10.1002/047002903X.

(65) Mizrahi Rodriguez, K.; Dean, P. A.; Guo, S.; Roy, N.; Swager, T. M.; Smith, Z. P. Elucidating the Role of Micropore-Generating Backbone Motifs and Amine Functionality on Membrane Separation Performance in Complex Mixtures. *Submitted* **2023**.

(66) Lou, Y.; Hao, P.; Lipscomb, G. NELF Predictions of a Solubility-Solubility Selectivity Upper Bound. *J. Membr. Sci.* **2014**, *455*, 247–253. https://doi.org/10.1016/j.memsci.2013.12.071.

(67) Yi, S.; Ghanem, B.; Liu, Y.; Pinnau, I.; Koros, W. J. Ultraselective Glassy Polymer Membranes with Unprecedented Performance for Energy-Efficient Sour Gas Separation. *Sci. Adv.* **2019**, *5* (5), eaaw5459. https://doi.org/10.1126/sciadv.aaw5459.

(68) Deng, J.; Huang, Z.; Sundell, B. J.; Harrigan, D. J.; Sharber, S. A.; Zhang, K.; Guo, R.; Galizia, M. State of the Art and Prospects of Chemically and Thermally Aggressive Membrane Gas Separations: Insights from Polymer Science. *Polymer* **2021**, *229* (June), 123988. https://doi.org/10.1016/j.polymer.2021.123988.

(69) Koros, W. J.; Paul, D. R.; Huvard, G. S. Energetics of Gas Sorption in Glassy Polymers. *Polymer* **1979**, *20* (8), 956–960. https://doi.org/10.1016/0032-3861(79)90192-7.

(70) Said, R. Ben; Kolle, J. M.; Essalah, K.; Tangour, B.; Sayari, A. A Unified Approach to CO_2-Amine Reaction Mechanisms. *ACS Omega* **2020**, *5* (40), 26125–26133. https://doi.org/10.1021/ACSOMEGA.0C03727/SUPPL_FILE/AO0C03727_SI_001.PDF.

(71) Gelles, T.; Lawson, S.; Rownaghi, A. A.; Rezaei, · Fateme. Recent Advances in Development of Amine Functionalized Adsorbents for CO_2 Capture. *Adsorption* **123AD**, *26*, 5–50. https://doi.org/10.1007/s10450-019-00151-0.

(72) Pate, S. G.; Xu, H.; O'Brien, C. P. Operando Observation of CO2transport Intermediates in Polyvinylamine Facilitated Transport Membranes, and the Role of Water in the Formation of Intermediates, Using Transmission FTIR Spectroscopy. *J. Mater. Chem. A* **2022**, *10* (8). https://doi.org/10.1039/d1ta10015g.

(73) Xu, H.; Pate, S. G.; O'Brien, C. P. Mathematical Modeling of CO_2 Facilitated Transport across Polyvinylamine Membranes with Direct Operando Observation of Amine Carrier Saturation. *Chem. Eng. Journ.* **2023**, *460* (January), 141728. https://doi.org/10.1016/j.cej.2023.141728.

(74) Tong, Z.; Ho, W. S. W. Facilitated Transport Membranes for CO_2 Separation and Capture. *Sep. Sci. Technol. (Philadelphia)*. 2017. https://doi.org/10.1080/01496395.2016.1217885.

(75) Tong, Z.; Ho, W. S. W. New Sterically Hindered Polyvinylamine Membranes for CO_2 Separation and Capture. *J. Membr. Sci.* **2017**, *543*. https://doi.org/10.1016/j.memsci.2017.08.057.

(76) Zhao, Y.; Winston Ho, W. S. Steric Hindrance Effect on Amine Demonstrated in Solid Polymer Membranes for CO_2 Transport. *J. Membr. Sci.* **2012**, *415–416*, 132–138. https://doi.org/10.1016/j.memsci.2012.04.044.

(77) Didas, S. A.; Sakwa-Novak, M. A.; Foo, G. S.; Sievers, C.; Jones, C. W. Effect of Amine Surface Coverage on the Co-Adsorption of CO_2 and Water: Spectral Deconvolution of Adsorbed Species. *J. Phys. Chem. Letters* **2014**, *5* (23), 4194–4200. https://doi.org/10.1021/jz502032c.

(78) Quan, W.; Wang, X.; Song, C. Selective Removal of H2S from Biogas Using Solid Amine-Based "Molecular Basket" Sorbent. *Energy and Fuels* **2017**, *31* (9), 9517–9528. https://doi.org/10.1021/acs.energyfuels.7b01473.

(79) Okonkwo, C. N.; Lee, J. J.; De Vylder, A.; Chiang, Y.; Thybaut, J. W.; Jones, C. W. Selective Removal of Hydrogen Sulfide from Simulated Biogas Streams Using Sterically Hindered Amine Adsorbents. *Chem. Eng. Journ.* **2020**, *379*. https://doi.org/10.1016/j.cej.2019.122349.

(80) Okonkwo, C. N.; Fang, H.; Sholl, D. S.; Leisen, J. E.; Jones, C. W. Effect of Humidity on the Sorption of H_2S from Multicomponent Acid Gas Streams on Silica-Supported Sterically Hindered and Unhindered Amines. *ACS Sustain. Chem. Eng.* **2020**, *8* (27). https://doi.org/10.1021/acssuschemeng.0c02012.

(81) Miller, D. D.; Chuang, S. S. C. The Effect of Electron-Donating Groups and Hydrogen Bonding on H_2S Capture over Polyethylene Glycol/Amine Sites. *J. Phys. Chem. C* **2016**, *120* (2). https://doi.org/10.1021/acs.jpcc.5b11796.

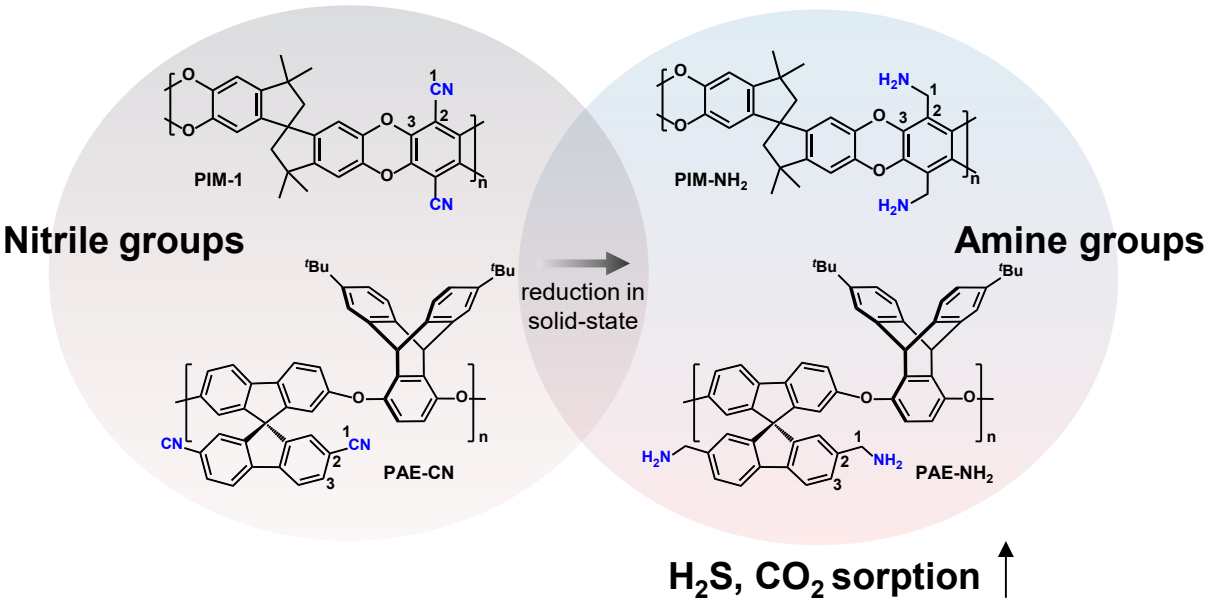
PIM-1
PIM-NH2
Nitrile groups
Amine groups
reduction in
solid-state
PAE-CN
PAE-NH2
H2S, CO2 sorption